

# Seismic performance of precast shear wall-slab connection under cyclic loading: experimental test vs. numerical analysis

Arthi S<sup>†</sup> and Jaya KP<sup>‡</sup>

*Department of Civil Engineering, Anna University, Chennai 600025, India*

**Abstract:** The structural behaviour of precast shear wall-diaphragm connection was compared with the monolithic connection under seismic loading. The monolithic connection was made by using U-bars connecting shear wall and slab, and the precast connection was made by using dowel bars in two steps. Firstly, U-shaped dowel bars from the precast shear wall lower panel and precast slab were connected by the longitudinal reinforcement, and screed concreting was done above the precast slab. Secondly, the shear wall upper panel was connected using the dowel bar protruding from the shear wall lower panel. The gap between the dowel bars and the duct was filled with non-shrink grout. The specimens were subjected to reverse cyclic loading at the ends of the slab. This study also aimed to develop a 3-D numerical model using ABAQUS software. The non-linear properties of concrete were defined by using the concrete damaged plasticity (CDP) model to analyse the response of the structure. The precast dowel connection between the shear wall and slab showed superior performance concerning ductility, strength, stiffness and energy dissipation. The developed finite element model exactly predicted the behaviour of connections as similar to that of experimental testing in the laboratory. The average difference between the results from finite element analysis and experimental testing was less than 20%. The results point to the conclusion that the shear resistance is provided by the dowel bars and the stiffness of the precast specimen is due to the diaphragm action of the precast slab. The damage parameter and the interaction between structural members play a crucial role in the modelling of precast connections.

**Keywords:** precast shear wall with the nib; diaphragm; dowel bars; concrete damaged plasticity; cohesive, reverse cyclic loading; hysteresis behaviour

## 1 Introduction

In recent years precast construction technology has progressively increased and been employed in a variety of structural applications. The process of assembling the precast elements into a structure is known as precast system. Prefabricated structures reduce the need for site formwork and labour cost and speed up the construction process with good quality. The seismic performance of precast structures entirely depends on the behaviour of connections, which are considered to be the weakest link in precast concrete construction. The design and construction of the connection between these precast structural elements is a big challenge. Improper detailing of connections between the various precast structural members leads to joint failure. It is therefore necessary to come up with practical connection detailing for precast concrete structures that has desirable seismic

performance compared to monolithic structures.

Shear wall plays a vital role in resisting the lateral load in structures. In previous research on various connection detailing between shear wall and slab, it has been shown that maximum stress concentration occurs at the shear wall-slab junction subjected to ground motions (Kaushika and Dasgupta, 2015) and slab got damaged near to the wall – slab junction for less vertical reinforcing bars in the wall (Kaushika and Dasgupta, 2019). Much work has been done on the seismic performance of monolithic connection between shear wall and slab using U-bars, additional bars, crossbars and stirrups connecting the U-bar (Greeshma and Jaya, 2008, 2011, 2012; Greeshma *et al.*, 2012; Surumi *et al.*, 2015b).

Prefabricated structure connections consist of two types: wet and dry. In situ concrete joints were used extensively in the early development of precast structures due to their simplicity of manufacture and rapid site progress (Elliot, 2017). Hutchinson *et al.* (1991) experimentally investigated the behaviour of post-tensioned horizontal connections between the precast shear wall and hollow-core floor slabs subjected to monotonic shear loading. The shear capacity of the proposed connection increases with the increase of load normal to the connection, and the failure of the connection supporting hollow-core slab is controlled

**Correspondence to:** Jaya KP, Department of Civil Engineering, Anna University, Chennai 600025, India  
Tel: +91-044 2235 7408

E-mail: [kpjaya@nayan.co.in](mailto:kpjaya@nayan.co.in), [jayakp@annauniv.edu](mailto:jayakp@annauniv.edu)  
<sup>†</sup>Research Scholar; <sup>‡</sup>Professor

**Supported by:** Council of Scientific and Industrial Research (CSIR)-SRF under Award Letter No. 09/468/0494/2016 EMR-I

**Received** October 29, 2018; **Accepted** May 5, 2019

by friction resistance and the shear capacity of the hollow-core slab. The shear strength of connection also depends on the loss of bond between the concrete fill and the hollow-core slab. Zhao *et al.* (2014) carried out an experimental study on precast shear wall with different details of hollow core slabs subjected to cyclic loads. In order to study the effect of different detailing of hollow core slab in the mechanical behaviour of precast shear wall hollow core structure, two types of hollow core slab (1 and 2) were designed. In type 1, the bidirectional holes of the hollow-core slab were circular, and the diameter of transverse holes was less than that of longitudinal holes. In type 2, the transverse and longitudinal holes remained square and circular respectively; the side-length of the transverse holes was larger than the diameter of the longitudinal holes. The authors observed that vertical macro cracks developed for specimen 1 and 2 along the weakest portion of concrete between longitudinal holes before peak value and along longitudinal distributed reinforcement in the precast hollow slab after peak value, respectively. Lu *et al.* (2018) carried out an experimental work to study the seismic behaviour of precast RC frame with shear wall. The base joints of shear wall was made by using reinforcement and post-tensioned tendons. It was observed that the unbonded PT tendons and the shear wall provided the restoring force and lateral force resistance respectively. Han *et al.* (2019) studied the seismic performance of precast hollow shear wall joints using lap splices of reinforcement. It was observed that the wall failed in shear mode.

In the case of cast-in-place connections, the shear acting at the joint region is taken care of by the dowel bars provided for connecting the precast structural members. Soudki *et al.* (1996) carried out the experimentation on horizontal connections between precast wall panels. The connection between two precast wall panels was made by using mild steel reinforcement, post-tensioning and shear keys. Rossley *et al.* (2014) proposed a connection using loop bars between interior and exterior precast concrete walls. The use of loop bars in the connection between precast concrete walls showed ductile behaviour and had greater moment carrying capacity. Vaghei *et al.* (2017) developed a new precast connection between precast wall panels and tested it under cyclic loading. The connection was made by using two steel channels connected by bolts and nuts. The proposed detailing showed higher energy dissipation and improved the resistance in all directions.

Joshi *et al.* (2005) compared the behaviour of the precast beam-column connection with the monolithic connection under cyclic loading. The precast connection at the joint region was made by welding the reinforcement bars. The authors concluded that the joint detailing with the beam bars welded to the column was recommended for earthquake resistant precast structures in high seismic zones. Seifi *et al.* (2015) carried out the experimental programme to study the seismic behaviour of the precast wall connected to the foundation using

grouted connection subjected to lateral loading. In this study, the connection was made by connecting 90-degree standard hook bars protruded from the foundation to the housing provided in the precast wall using metal duct, and then the gap was filled with grout. The gap between the precast wall and foundation were dry packed. The proposed grouted connection between precast wall and foundation showed a ductile behaviour with maximum strength 10% larger than the design flexural capacity of the connection.

Numerical modelling of the precast dowel connection between structural members was done using the finite element software ABAQUS to simulate the seismic response of the connection. The dowels embedded in the column were inserted into the housing provided in the beam, and then the gap was filled with mortar (Magliulo *et al.*, 2014; Kremmyda *et al.*, 2013). The Concrete Damaged Plasticity (CDP) model can be used to define the non-linear behaviour of concrete in ABAQUS (Surmi *et al.*, 2015a; Alfarah *et al.*, 2017). It is important to define the models for the non-linear property of materials and the interaction between the precast connections (Zoubek *et al.*, 2014). Many research works related to seismic behaviour of precast connections such as beam-column, column-foundation, wall-wall, etc. have been available (Rahman *et al.*, 2006; Ketiyot and Hansapinyo, 2018; Zenunovic and Folic, 2012; Feng *et al.*, 2016; Fischinger *et al.*, 2012; Yuksel *et al.*, 2015). However, the works related to precast shear wall-slab dowel connection with ductile detailing is minimal. It is therefore necessary to investigate the structural behaviour of the precast shear wall-slab connection subjected to seismic loading.

## 1.1 Novelty of the study

From the literature review, it is observed that the detailing of precast connection can be as ductile as that of monolithic connection. It has also been observed that much research has been done on the precast connection between different structural members using dowel bars. The existing databases of tested specimens of precast shear wall-diaphragm connection detailing are very limited, and only a few numerical studies on precast connections have been reported to date. There are no particular guidelines available in the Indian Codes of practice for the detailing between precast shear wall-diaphragm connections. The present research work aimed to develop precast ductile detailing of connection between shear wall and slab using dowel bars and to compare its hysteresis behaviour with that of a reference monolithic connection. Therefore, monolithic and precast specimens were cast and tested experimentally. The present study compared the structural performance of ductile detailing of precast specimen subjected to reverse cyclic loading with that of monolithic connection.

## 1.2 Objective

The primary objectives of the present study are as

follows:

(1) To conduct an experimental investigation of precast and reference monolithic connection.

(2) To compare the structural performance of the precast connection with that of the monolithic shear wall-diaphragm connection subjected to reverse cyclic loading.

(3) To develop a 3D numerical model of precast shear wall-diaphragm connection using ABAQUS software and to compare the numerical results with the tested specimen.

## 2 Experimental work

### 2.1 Design criteria

An eight-story RC precast building located in Chennai was taken to study the performance of shear wall-slab connection under reverse cyclic loading. STAAD PRO software was used for the modelling and analysis of this structure. The resultant forces around the exterior shear wall-slab joint due to different load combinations defined as per IS 1893 part (1)-2002 were computed. The critical design forces such as shear force, bending moment, and axial load are 963.04 kN, 2520.48 kN-m, and 1757.11 kN respectively. The design and detailing of shear wall and the slab was done as per IS 456-2000 and IS 13920-1993 respectively. Both specimens were cast with one-third scaled down model. The dimensions of both the monolithic and precast specimens are shown in Table 1.

#### 2.1.1 Monolithic specimen (MS)

The reinforced concrete MS was designed as per IS 456-2000 and detailed as per IS 13920-1993. The reinforcement detail is shown in Fig. 1(a). The connection was provided by using U-bar in the joint region and was extended into the slab by the development length ( $L_d$ ) of 270 mm from the face of the shear wall, which was calculated as per IS 456-2000.

#### 2.1.2 Precast specimen (PS)

The precast specimen consisted of three parts: shear wall - lower panel with nib, upper panel, and precast slab with in-situ concrete topping. The connection between

the shear wall lower panel to the upper panel and the slab was provided with dowel bars protruding from the lower panel as shown in Fig. 1(b). The reinforcement detail is shown in Fig. 1(b). Four 6 mm diameter dowel bars were used to connect the shear wall and slab, out of which two U-shaped bars projected from the lower panel and the other two from the precast slab. The longitudinal reinforcement connected these four U-shaped dowel bars. Mesh reinforcement was provided above the precast slab and in situ concrete topping was done in order to maintain the diaphragm action of the structure. The upper panel was provided with a duct to create a housing for inserting the dowel from the lower panel. The gap between the duct and dowel was filled with high strength, non-shrink M-60 grade grout. The diameter of the duct provided in the upper panel for inserting the dowels protruding from the lower panel was 20 mm, and the diameter of the dowel bars for the connection between upper panel - lower panel was 10 mm. The development length of dowel bars for wall and slab was 450 mm and 270 mm, respectively. The dowel design was based on the guidelines given by Elliot (2017). The erecting stages of the precast specimen are shown in Table 2.

### 2.2 Material properties

M-30 grade concrete and HYSD bars of Fe-500 grade steel was used for casting the specimens. The average 28 days compressive strength ( $f_{ck}$ ) of the concrete by testing three cubes of 150 mm × 150 mm × 150 mm was found to be 39.4 N/mm<sup>2</sup>. The average tensile strength ( $f_{ct}$ ) of the concrete from testing three cylinders of 150 mm diameter and 300 mm height was obtained as 3.21 N/mm<sup>2</sup>.



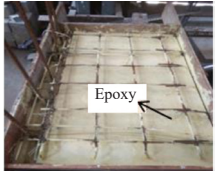
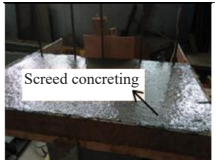



### 2.3 Experimental test set up

The typical ground storey exterior shear wall-slab joint region was considered as the test specimen for the experimental investigation. The specimen was comprised of (i) ground storey shear wall, (ii) ground floor roof slab up to the mid portion, (iii) first storey shear wall up to the mid-height. Due to the lateral loading, the exterior shear wall-slab sub assemblage was subjected to the in-plane moment at the joint region. The in-plane moment was

**Table 1** Dimensions of the one-third scaled down specimen

No.	Type of specimen	Structural members	Length (mm)	Width (mm)	Depth (mm)
1	Monolithic	Shear wall	800	80	1550
		Slab	800	430	60
2	Precast	Shear wall-lower panel	800	80	1000
		Projecting nib in the lower panel	800	110	100
		Precast slab	800	430	30
		Screed concrete	800	430	30
		Shear wall-upper panel	800	80	500

**Table 2 Construction sequence of precast specimen**

No.	Assembly sequence	Figure
1	The shear wall-lower panel was fixed in the frame.	
2	The precast slab was placed, and the dowels from the precast slab were bent and tied with the mesh reinforcement. The longitudinal reinforcement connects these four U-shaped dowel bars.	
3	Epoxy was applied before casting the screed concrete for the proper bonding between the concrete cast at different times.	
4	Screed concreting was done and then cured.	
5	Dowels protruding from the shear wall-lower panel were inserted into the housing provided in the shear wall-upper panel. The shear wall-upper panel was erected.	
6	Grouting was done as infill for the gap between dowels and duct provided in the shear wall-upper panel while casting.	
7	Final erected stage of the specimen.	

simulated for the experimental testing through a couple of forces acting at the slab ends as shown in Fig. 2(a). In order to simulate the effects of dead load, concrete cubes were arranged at the top of the projecting slab throughout the test. Two double-acting hydraulic jacks were mounted on the loading frame at the bottom side of the slab for the application of reverse cyclic loads. The experimental test set up is shown in Fig. 2(b). The test was carried out under a displacement controlled loading concept. The bottom of the shear wall was fixed to the strong floor. In order to counter the effects of gravity load from the above stories, gravity load was chosen as 10%

of the load-bearing capacity of the wall and was applied at the top of the projecting slab. Three cycles were applied for each displacement level. The reverse cyclic loading was applied to the specimens according to ACI T1.1-01 (Feng *et al.*, 2016). The loading protocol used in this study is shown in Fig. 2(c). This loading protocol was used in this study because it uses displacement control method for loading the specimens. The criteria for this displacement control loading protocol include the following:

(1) The initial drift ratio should be within the elastic range. The subsequent drift ratios should be values not

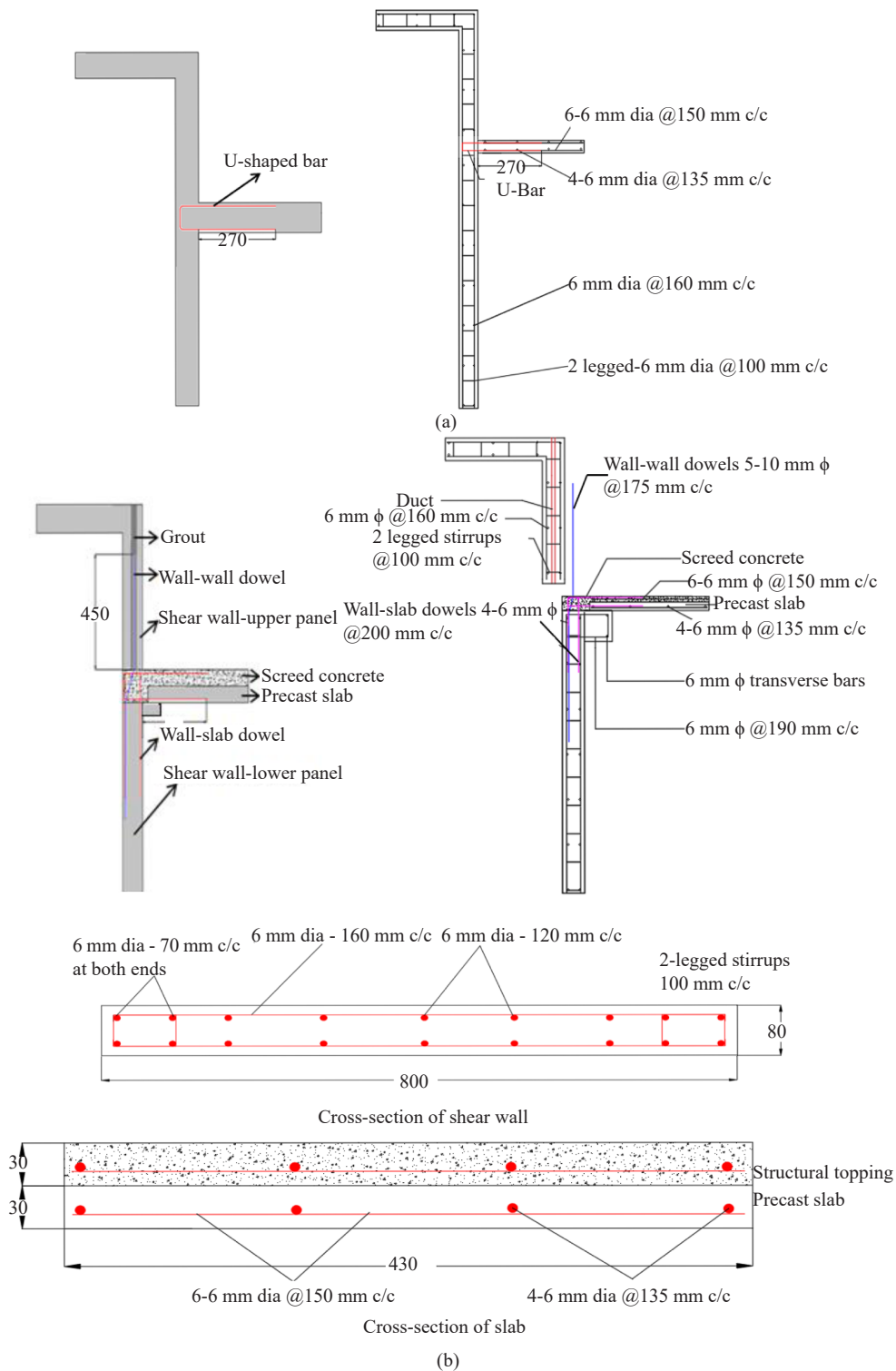


Fig. 1 Reinforcement detailing: (a) monolithic specimen, (b) precast specimen

less than one and one-quarter times, and not more than one and one-half times the previous drift ratio.

(2) Three cycles should be applied for each drift ratio.

(3) Loading should be continued until the drift ratios equal or exceed 3.5%.

### 3 Result discussion

#### 3.1 Crack pattern

The crack in the specimen opens and closes on reverse loading. Crushing and spalling of the concrete



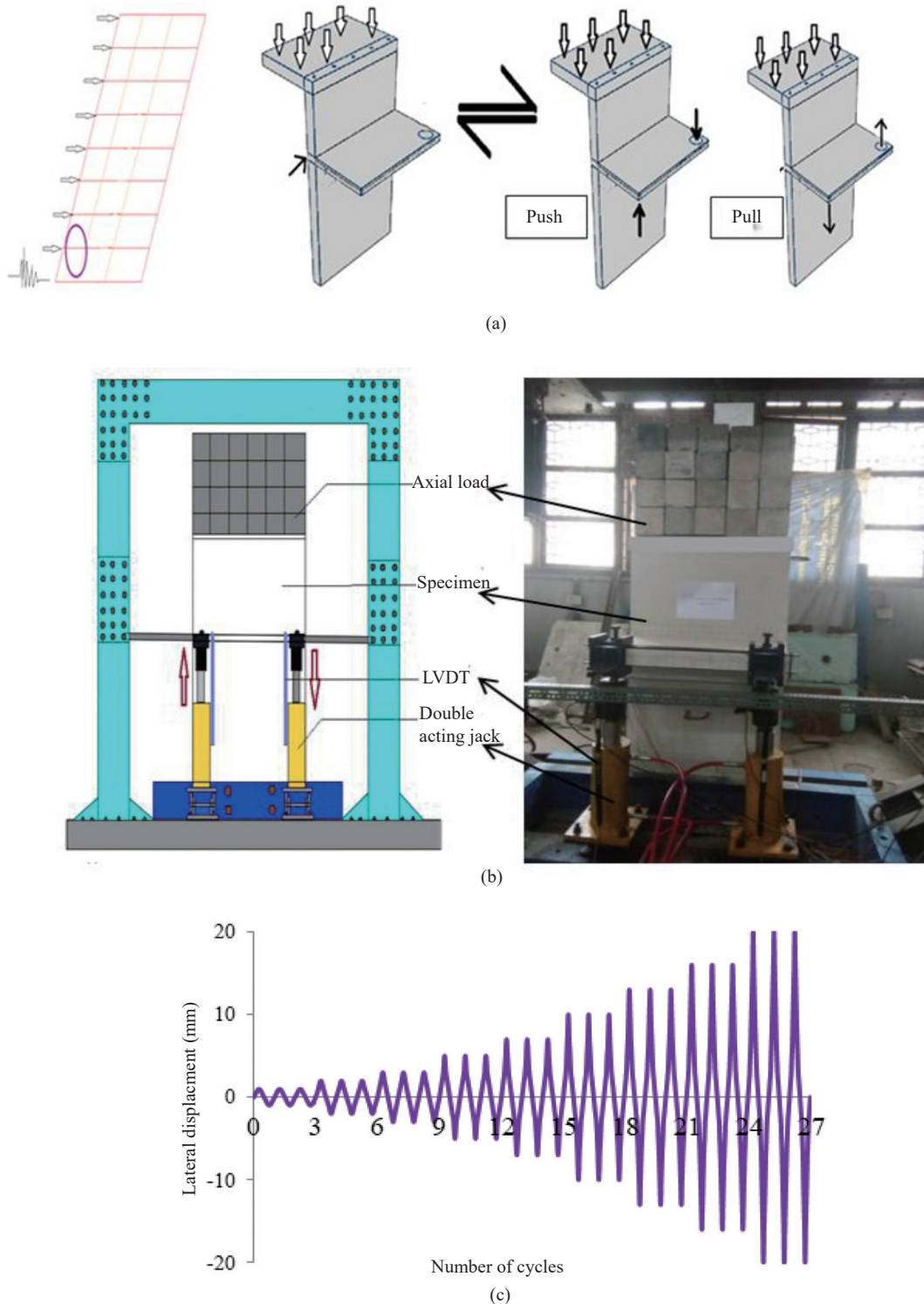


Fig. 2 (a) Loading simulation, (b) experimental set-up, (c) loading protocol

were observed at the slab ends near the loading region. In MS, the initial crack started in the slab portion at 2 mm (8.7 kN) displacement cycle, and the cracks propagated in the slab region as the displacement increased. These cracks extended in the slab diagonally and developed towards the joint region. At 5 mm (10.2 kN) positive displacement, visible shear cracks

were observed and widened in the joint region at 10 mm (10.9 kN) positive displacement. The maximum displacement reached by the MS was 20 mm, and the ultimate load carrying capacity of the MS reached at 10 mm displacement. In PS, the initial crack was observed at 5 mm (12.6 kN), and the shear crack extended as displacement

increased. The diagonal shear crack formed in the joint region at both ends of the slab. Cracks initiated at the interfaces between the structural members provided at the connection. A separation appeared between the precast lower panel-precast slab and the precast slab and screed concrete as displacement increased. Spalling of concrete was observed in the slab at 10 mm (13.2 kN) displacement. The separation between the screed concrete and precast slab started at 20 mm (14.3 kN). As displacement increased, a 12 mm gap appeared between the precast shear wall lower panel and the precast slab.

In both specimens, the shear cracks started from the loading point and extended diagonally in the slab region at both faces of the slab. The diagonal cracks extended towards the joint region as the displacement increased. No visible crack was observed in the shear wall, but in the PS, a minor crack was seen in the nib portion. The crack pattern of the monolithic and precast specimen is shown in Fig. 3.

### 3.2 Load-Displacement Relationship

The displacement controlled loading was applied at the ends of the slab at 410 mm away from the joint region. The load vs. displacement curve and the envelope curve have been plotted for both the specimens, as shown in Fig. 4. During the initial stage of loading, the hysteric behaviour of both specimens showed linear load-displacement response and later the pinching was observed in the hysteric loop of both specimens. The load-displacement hysteric response of the precast specimen is shown in Fig. 4(b). Greater pinching was observed for the precast specimen due to the predefined gap at the joint region. The increase in ultimate load and stiffness was observed in the PS due to the diaphragm action as compared with the MS. The presence of dowels bars connected by the longitudinal reinforcement at the connection increased the shear resistance in the joint region during both push and pull direction loading.

### 3.3 Strength

For MS, the ultimate strength was found to be 10.9 kN and 9.27 kN in the push and pull directions respectively. The ultimate strength for the PS in the push

direction was about 15.15 kN and in the pull direction was about 14.1 kN. The ultimate strengths of the MS and PS are shown in the Fig. 5. The PS shows 38.9% and 52.1% larger load-carrying capacity than the MS in the push and pull direction loading. The ultimate strength of the PS was found to be greater when compared with the MS due to the resistance offered by the dowel bars and the presence of the nib, which supports the precast slab. The dowel bars provided at the joint, and the diaphragm action of the precast slab, increased the shear resistance at the connection region.

### 3.4 Stiffness degradation

Reinforced concrete structures will exhibit some level of stiffness degradation when subjected to reverse cyclic loading. Stiffness degradation may be due to loss of bond, high-stress concentration or cracking. The level of stiffness degradation depends on the ductile detailing of structural members and its connections. In general, the stiffness of a structure is defined as the capacity of the structure to resist deformation under the applied load. In this study, the stiffness degradation of the test specimens was measured based on secant stiffness. The secant stiffness or peak-to-peak stiffness was measured by the slope connecting peak-to-peak positive and negative loading during each cycle (Saqa, 1995). The stiffness degradation of the tested specimens for each loading cycle is shown in Fig. 6.

As displacement increased, there was cumulative damage in the joint core and slab, which led to stiffness degradation of the connection. As seen in Fig. 6, it was observed that, in the inelastic stage, the precast specimen showed higher stiffness when compared with the monolithic specimen. The initial stiffness of the PS was 20.28% higher than the MS due to the diaphragm action provided by the precast slab.

### 3.5 Energy Dissipation

A connection proves to be ductile if an adequate amount of energy is dissipated by the joint region without strength and stiffness degradation. The energy dissipation was calculated by the area enclosed by the load vs. displacement curve in each displacement cycle.

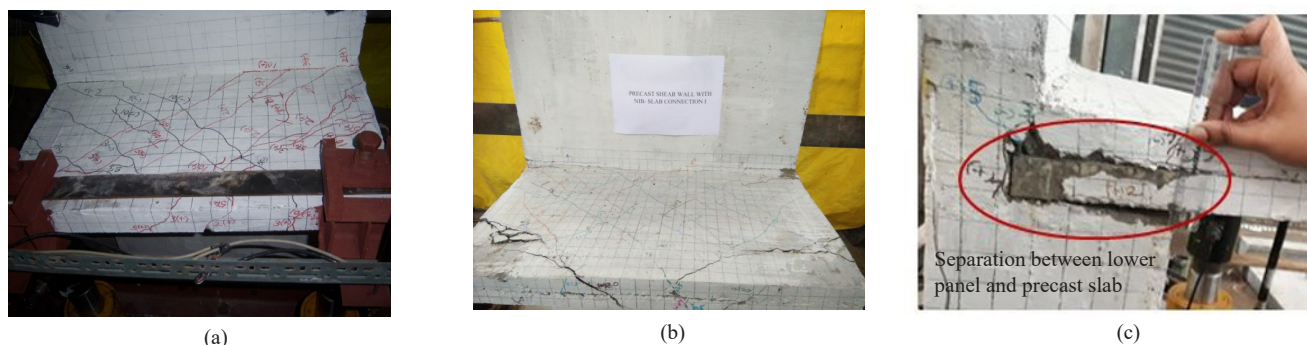


Fig. 3 Crack pattern: (a) monolithic specimen, (b) precast specimen, (c) separation of precast structural members

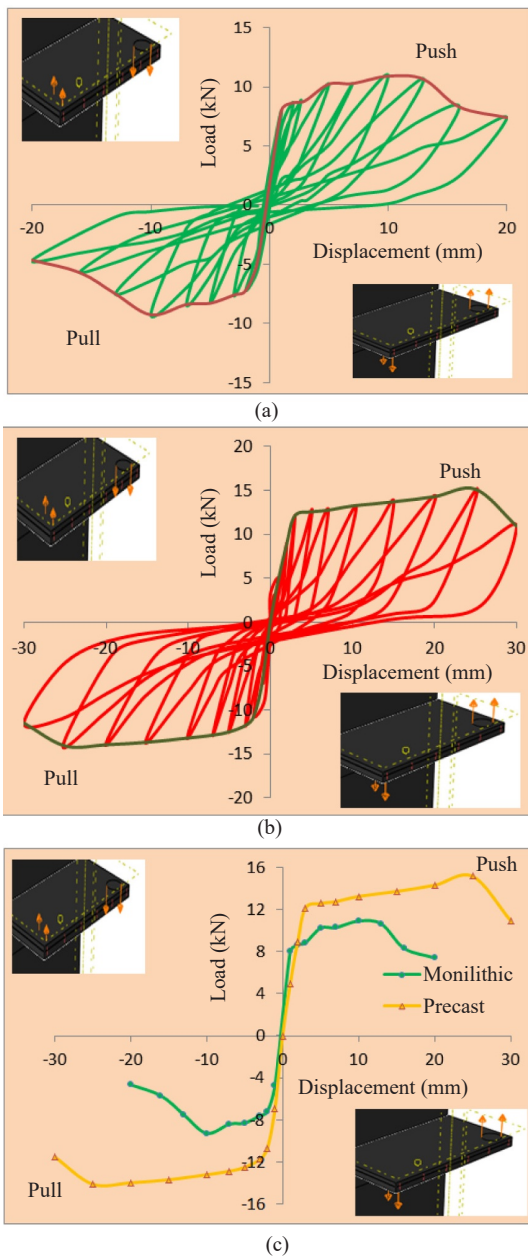


Fig. 4 Hysteresis graph: (a) monolithic specimen, (b) precast specimen, (c) envelope graph

The comparison of cumulative energy dissipation for both specimens is shown in Fig. 7. The area of the hysteresis loop in each displacement cycle becomes larger as displacement increases. The ultimate displacement of the precast specimen was 30 mm. The PS shows 126.9% larger energy dissipation in comparison with the MS.

### 3.6 Post-elastic strength enhancement factor

Load ratio, or post-elastic strength enhancement factor, indicates the development of the load carrying capacity beyond yield and the degree of degradation of the connection. It is obtained by the ratio of the maximum load during each cycle of displacement

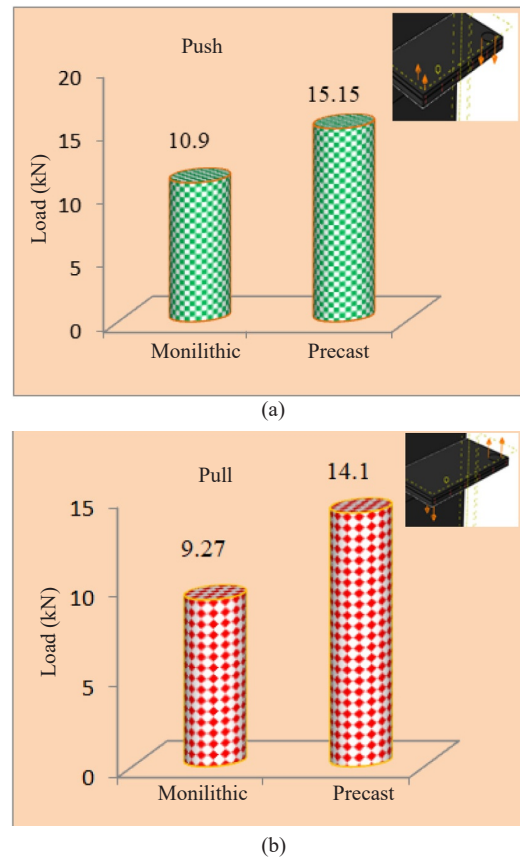


Fig. 5 Comparison of strength: (a) push direction, (b) pull direction

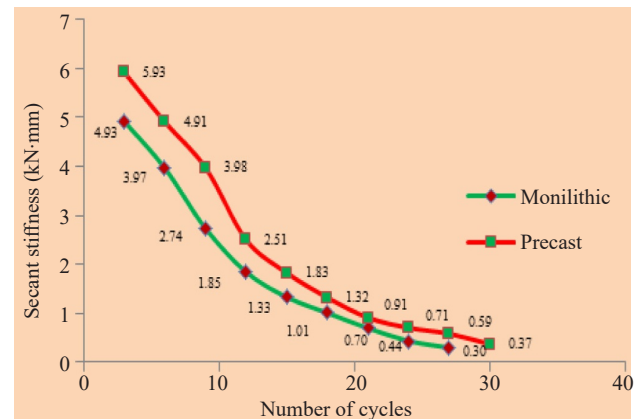


Fig. 6 Stiffness degradation at each cycle

and the yield load of the connection (Alameddine and Eshani, 1991). The average maximum load ratio for the MS and PS was found to be 1.31 and 1.25 respectively (Table 3). The maximum displacement reached by the MS and PS was 20 mm and 30 mm respectively. The precast specimen was able to maintain the yield load for all the loading cycles up to 7.3% drift. This load ratio is not observed in the MS. The MS showed a dropping trend beyond 2.5% drift. In comparison with the MS, the precast specimen showed less deterioration because of the good confinement in the connection region and



the diaphragm action of the precast slab. The load ratio was plotted against the corresponding displacement and is shown in Fig. 8.

### 3.7 Ductility

Ductility factor was calculated by the ratio of ultimate to yield displacement. Yield and ultimate displacement are the displacement corresponding to 80% of ultimate load in the ascending and descending branch from the envelope curve (Tawfik *et al.*, 2014). It was observed that both specimens behaved in a ductile manner. Table 4 shows the ductility factor of both specimens. The ductility for the PS was found to be 97.37 % greater than the MS. The higher ductility factor for the PS is a sign of satisfactory performance of the connection in the plastic (inelastic) stage.

### 3.8 Strains in reinforcement

In this study, strain gauges were used to measure the strain in reinforcement. Four electrical strain gauges were pasted at various locations, as shown in Fig. 9(a). The strain values corresponding to the lateral displacement of the specimens are shown in Fig. 9(b1) and Fig. 9(b2). As seen in Fig. 9(b), it was observed that, as displacement increased, all reinforcement bars experienced a continuous increase in strain. The strain at the joint region of the precast specimen was less than the strain at the joint region of the monolithic specimen. The strain in the top and bottom longitudinal bars of the slab was found to be higher than the strain at the joint region for both the monolithic and precast specimen, which shows slab mode failure.

## 4 Numerical simulations

Finite element modelling of both monolithic and precast shear wall-slab connections was done by using

the finite element software ABAQUS. This study analysed and predicted the seismic behaviour of both specimens subjected to reverse cyclic loading.

### 4.1 Modelling of specimens

A one-third scale model similar to the tested specimen was modelled, as shown in Fig. 10, and the

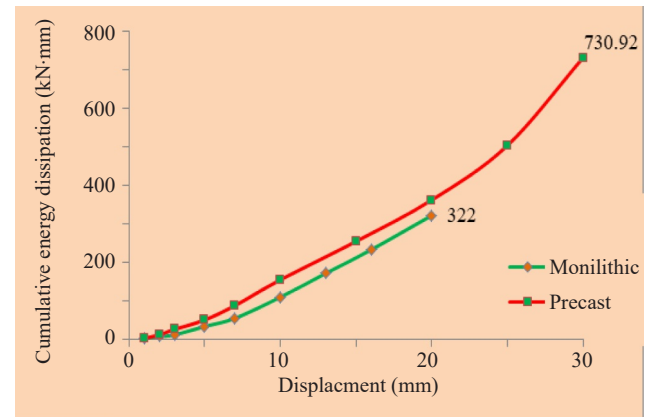


Fig. 7 Cumulative energy dissipation curve

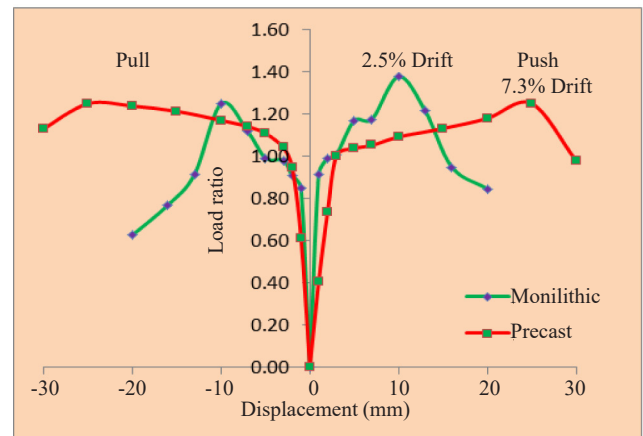


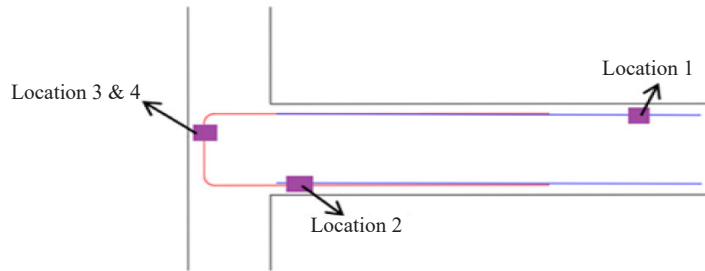
Fig. 8 Load ratio of both specimens

Table 3 Comparison of load ratio for both the specimen

No.	Drift ratio (%)	Displacement (mm)	Load ratio			
			Push direction		Pull direction	
			Monolithic	Precast	Monolithic	Precast
1	0.3	1	0.91	0.41	0.85	0.61
2	0.5	2	0.99	0.74	0.91	0.95
3	0.7	3	1.01	1.00	0.98	1.04
4	1.1	5	1.17	1.04	0.99	1.11
5	1.7	7	1.18	1.05	1.12	1.14
6	2.5	10	<b>1.38</b>	1.09	<b>1.25</b>	1.17
7	3.9	16	0.95	1.13	0.77	1.21
8	4.9	20	0.85	1.18	0.63	1.24
9	6.1	25	-	<b>1.25</b>	-	<b>1.25</b>
10	7.3	30	-	0.98	-	1.13

**Table 4 Comparison of ductility factor of precast and monolithic specimens**

No.	Specimen type	Yield displacement $\Delta_y$ (mm)		Ultimate displacement $\Delta_u$ (mm)		Ductility factor, $\mu$		Average ductility factor, $\mu$
		Push	Pull	Push	Pull	Push	Pull	
1	Monolithic	2.41	2.5	15.46	10.66	6.41	4.26	5.34
2	Precast	3.02	2.58	28.67	29.88	9.49	11.58	10.54



- Location 1: Strain in the top bar of the slab in left side
- Location 2: Strain in the bottom bar of the slab in right side
- Location 3: Strain in the connection (left side)
- Location 4: Strain in the connection (right side)

(a)

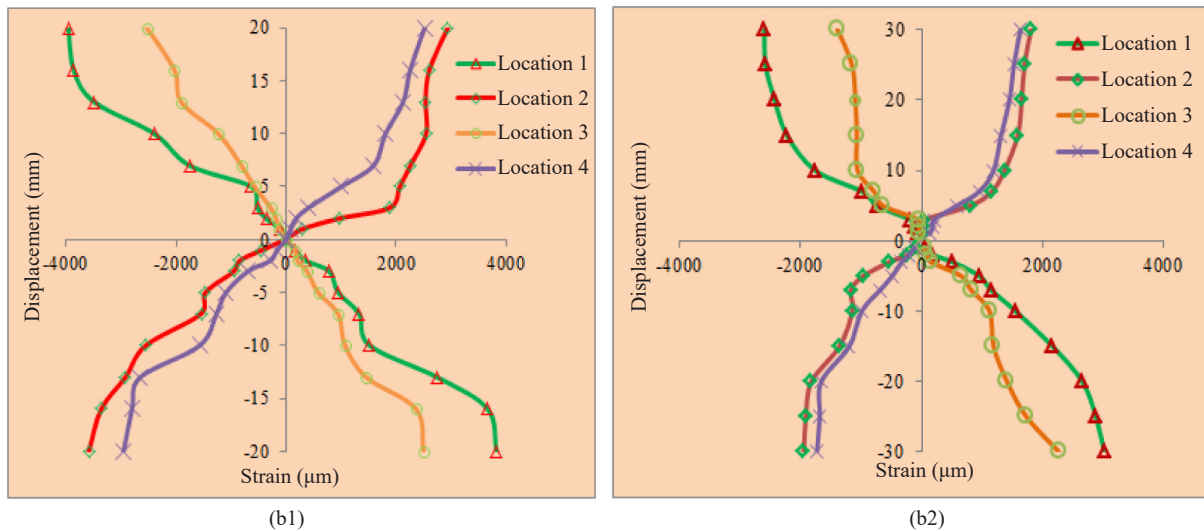


**Fig. 9 (a) Position of strain gauges, (b) strain response in reinforcement, (b1) monolithic specimen, (b2) precast specimen**

reinforcement detailing is shown in Fig. 11. In this study, an eight–node linear brick element (C3D8R) was chosen to model the concrete and grout part, and a two–node linear beam element (B31) with the circular profile of 6 mm diameter was used to model the reinforcement. The section properties of concrete and steel bars are shown in Table 5. The concrete and steel elements are meshed with the global size of 50 and 40 respectively.

**4.2 Material properties**

**4.2.1 Concrete**

In ABAQUS, the non–linear properties of concrete can be modeled in two ways: (a) Concrete Damaged

Plasticity (CDP) and (b) Smearred Cracking model. CDP was used to model the inelastic response of concrete material under reverse cyclic loading (Dere and Koroglu, 2017). The CDP model includes two types of failure mechanisms, namely compression (crushing) and tension (cracking) of concrete, and the response of concrete to cyclic loads in the CDP model is shown in Fig. 12(a). In addition, the CDP model includes the plasticity properties to define yield surface, potential flow and the viscosity parameter, as shown in Table 7. The damage parameter in the softening zone was also introduced in this CDP model in the tension and compression behaviour of the concrete material. The methodology used for calculating damage parameters was done as stated by Alfarah *et al.*

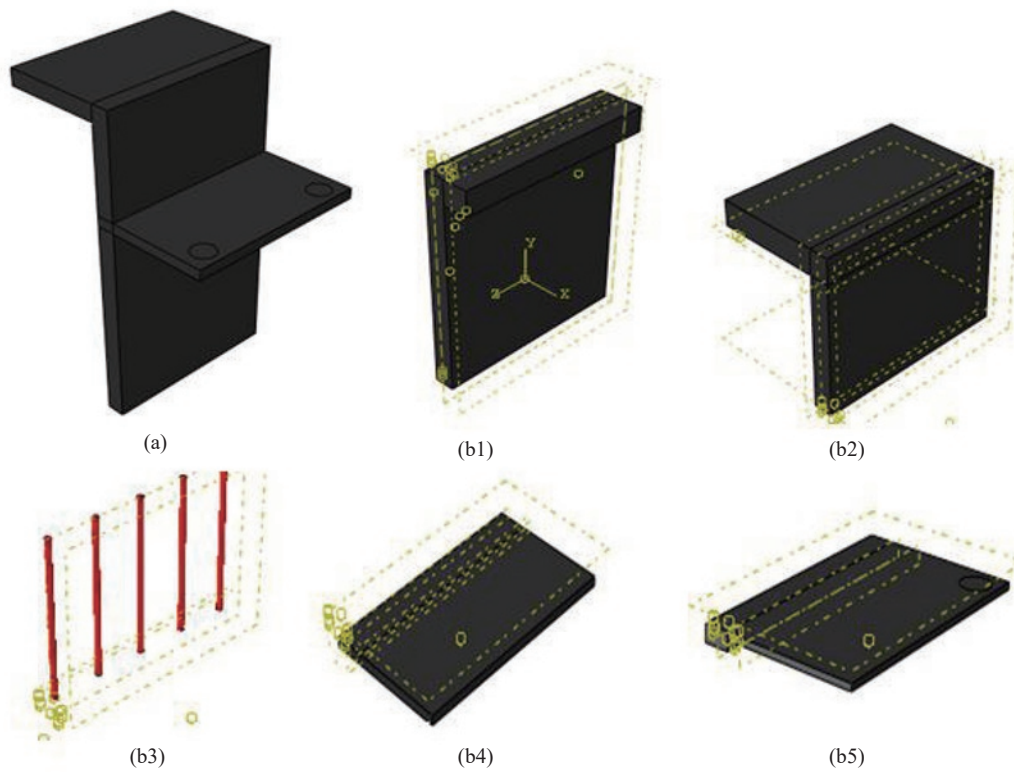


**Fig. 10** Parts in ABAQUS: (a) monolithic specimen, (b) precast specimen, (b1) shear wall lower panel with nib, (b2) upper panel, (b3) grouting in upper panel, (b4) precast slab, (b5) screed concrete

**Table 5** Sectional properties of elements

Properties	Concrete/Grout	Reinforcement
Model	3D-deformable	3D-deformable
Shape	Solid, Extrusion	Wire, planar
Section	Solid, homogeneous	Beam, circular profile
Mesh		
Element Library	Standard	Standard
Geometry	Linear	Linear
Family	3D stress	Beam
Element	C3D8R	B31

8 - node element

2 - node element

(2017), and the stress-strain curve in both compression and tension is shown in Fig. 12(b). The elastic properties of concrete and grout are shown in Table 6, and the material properties assigned to the model are shown in Fig. 12(d).

#### 4.2.2 Steel

The elastic modulus and poisson ratio of steel are

200000 N/mm<sup>2</sup> and 0.3, respectively. The plastic phase of steel was modelled using bilinear behaviour including yield stress and plastic strain (Fig. 12(c)).

#### 4.3 Interaction

In the monolithic specimen, the interaction between

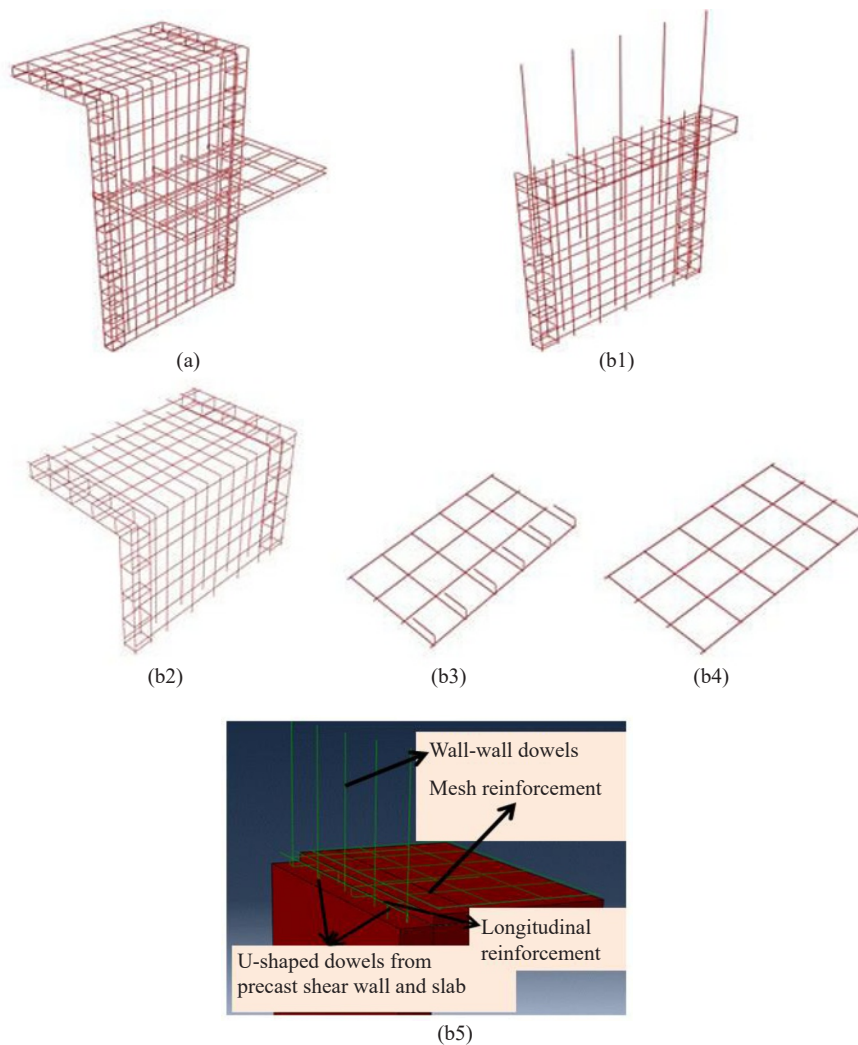


**Fig. 11 Reinforcement detailing: (a) monolithic specimen, (b) precast specimen in abaqus, (b1) shear wall lower panel with nib, (b2) upper panel, (b3) precast slab, (b4) screed concrete, (b5) joint detailing**

**Table 6 Elastic properties of concrete and grout**

Part	Concrete	Grout
Elastic modulus, $E$ (N/mm <sup>2</sup> )	32725.49	32000
Poisson ratio	0.2	0.2

**Table 7 Plasticity properties in CDP model**

No.	Description	Value
1	Dilation angle	38
2	Eccentricity	0.1
3	Initial/Biaxial stress ratio	1.12
4	$K$	0.67
5	Viscosity parameter	0.666

concrete and steel was assumed to have the full bond, and therefore it was modelled using an embedded region constraint. The precast specimen includes three

interaction regions, namely shear wall lower panel-precast slab, precast slab-screed concrete, and screed concrete-upper panel. A tie constraint was used between screed concrete and the upper panel, since there was no debonding between the surfaces observed during testing. A debonding was observed between the precast slab-screed concrete and the lower panel-precast slab during experimental testing. Therefore, an 8-noded three-dimensional cohesive element COH3D8 was used to define the interaction between the precast structural members (Fig. 13). The cohesive element of 1 mm thickness was created in the shear wall lower panel and precast slab. The interaction between the elements was defined by stiffness, fracture energy and shear stress at the interface (Obaidat *et al.*, 2010; Fib, 2013).

#### 4.4 Boundary conditions and analysis

The boundary conditions were applied to the model similar to the experimental programme. The shear wall was fixed at the bottom. The axial load was applied at the



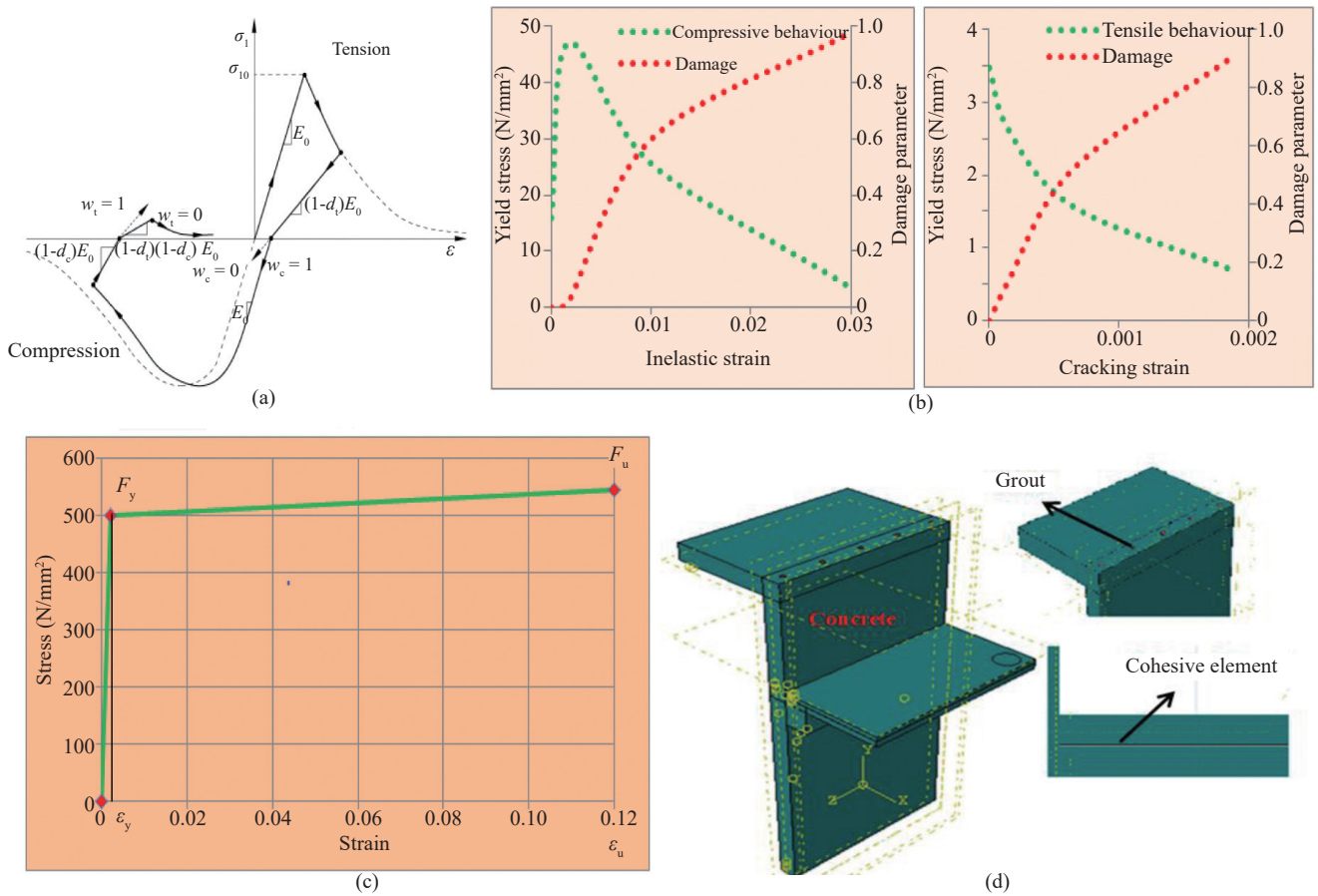


Fig. 12 (a) Response of concrete to cyclic loads, (b) stress-strain curve of CDP model (compression and tension), (c) stress-strain curve of steel, (d) material property assigned to the model

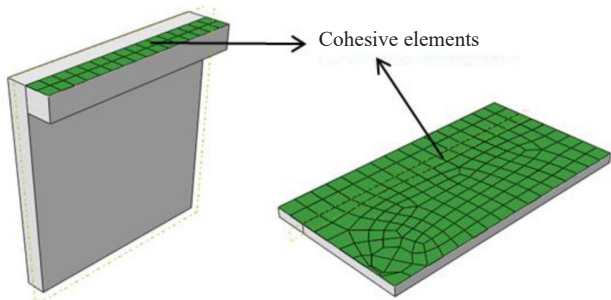


Fig. 13 Cohesive element at the interface in the precast specimen

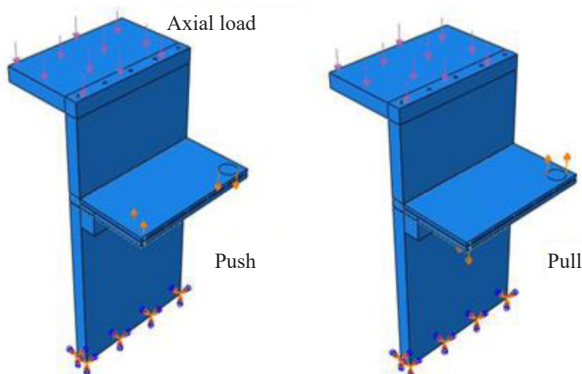


Fig. 14 Boundary conditions

top of the projecting slab of the specimen. The circular shape partition cell was created at the slab ends for the application of reverse cyclic loading. The displacement controlled loading was applied at the partition cell. The reverse cyclic loading was applied as a smooth step amplitude function, and the analysis was carried out in two steps. The first step dealt with the axial load and the second step showed the response for cyclic load in addition to axial load (Fig. 14).

## 5 Numerical results

### 5.1 Visualization

The maximum deformation of precast and the monolithic specimen in the push and pull direction was found to be 30 mm and 20 mm respectively. The deformed shape of both the monolithic and the precast specimen subjected to reverse cyclic loading exhibited similar deformation behaviour when compared to experimental observations, and it is shown in the Fig. 15. The damage pattern of both specimens is shown in Fig. 17. It was observed that the use of cohesive elements at the interface in the developed model accurately predicts the debonding between the precast shear wall-slab and the

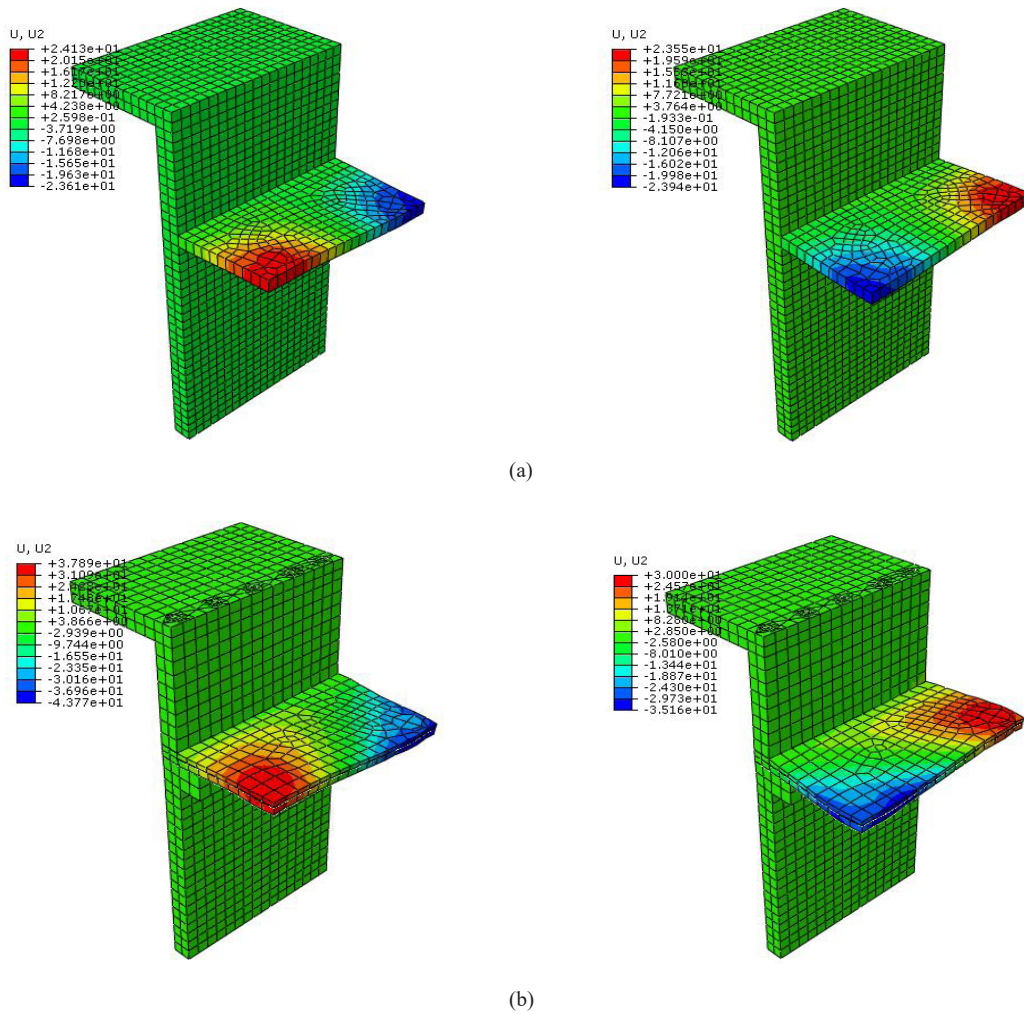


Fig. 15 Deformation: (a) monolithic specimen, (b) precast specimen

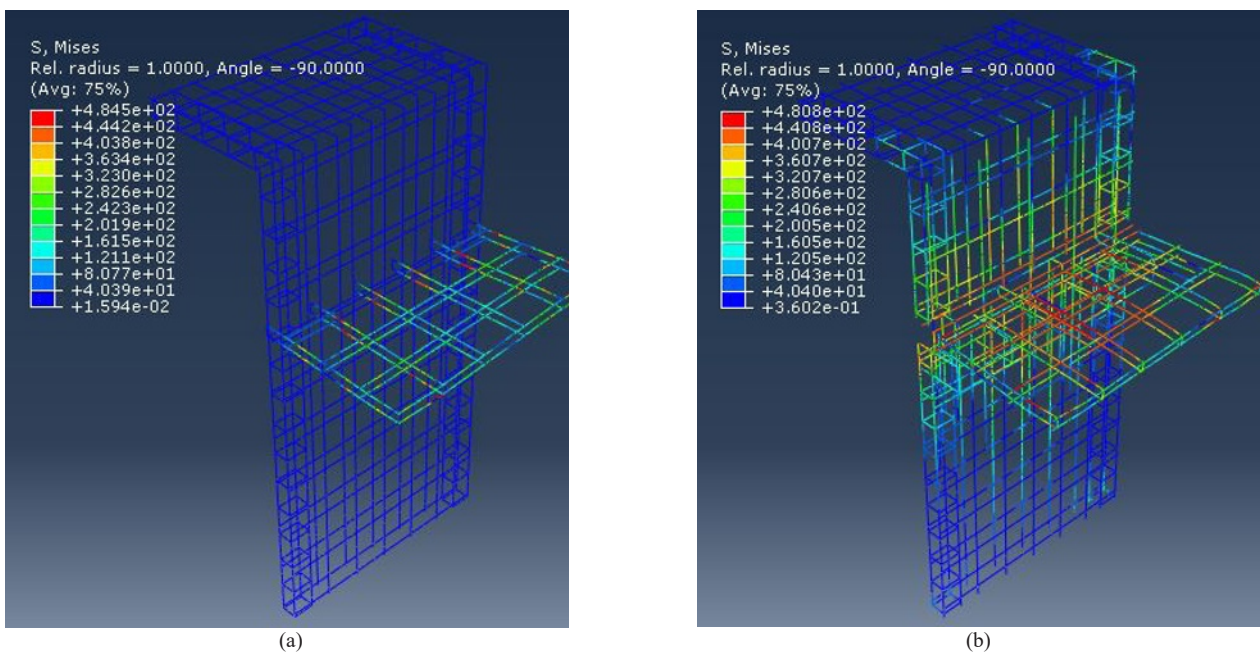
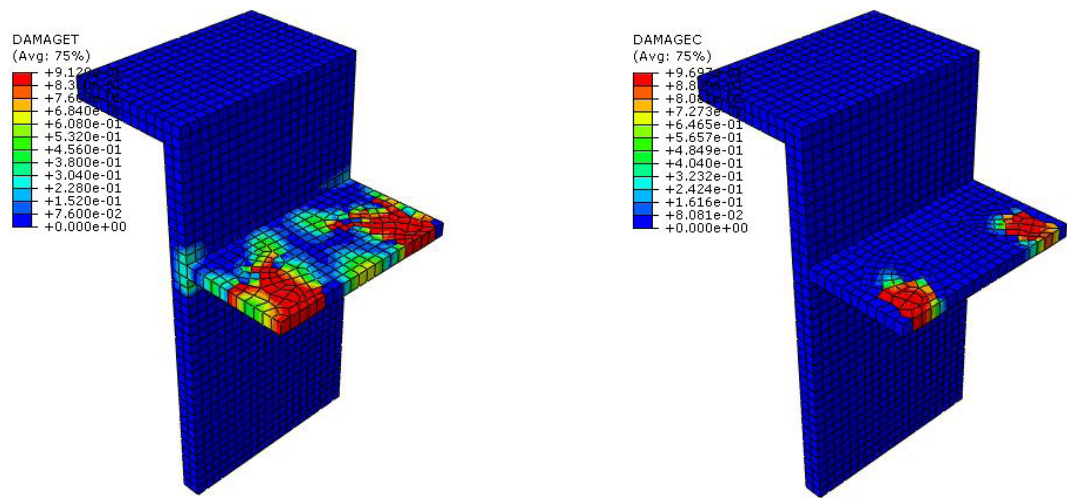
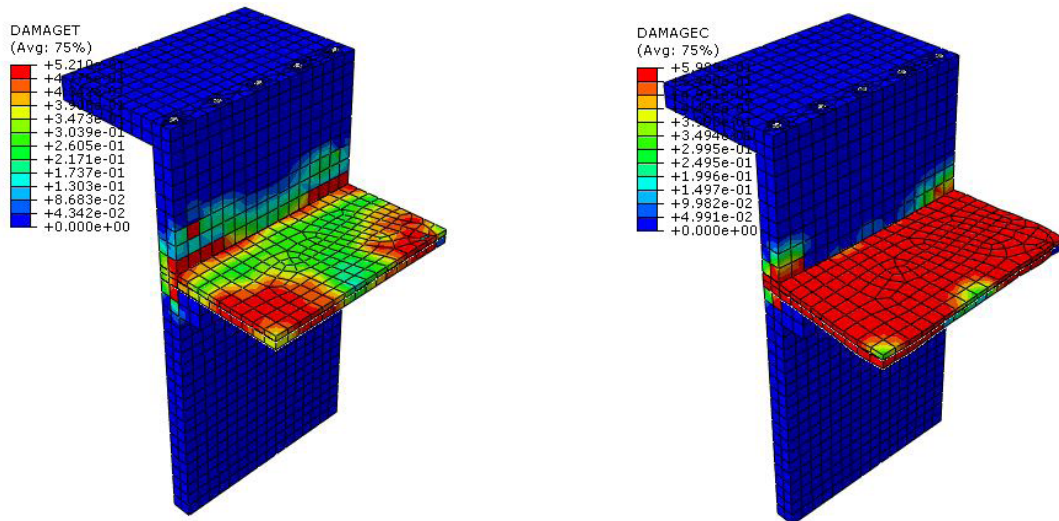


Fig. 16 Strain in reinforcement: (a) monolithic specimen, (b) precast specimen



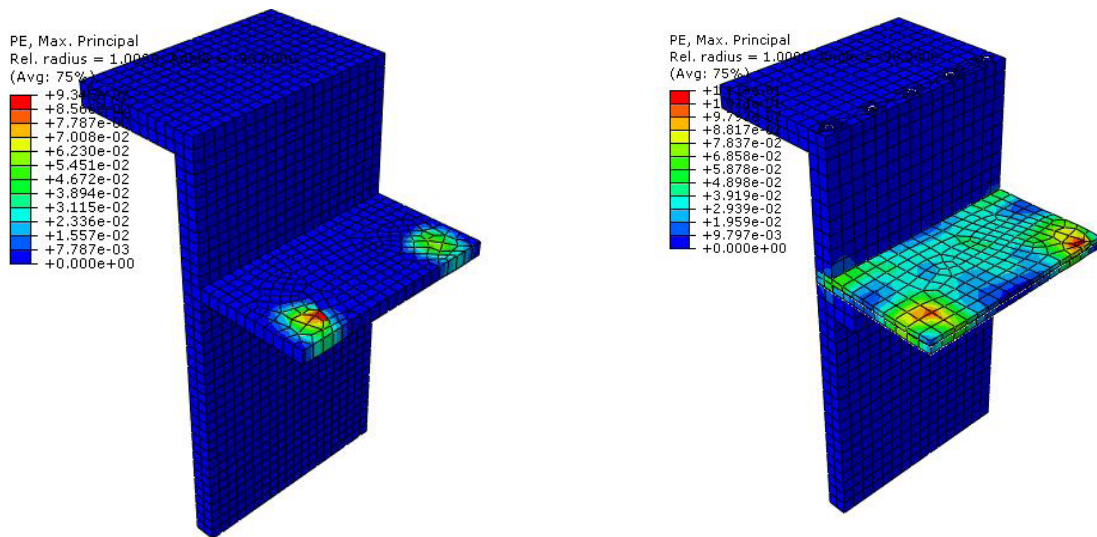


(a)



(b)

Fig. 17 Damage in compression and tension: (a) monolithic specimen, (b) precast specimen



(a)

(b)

Fig. 18 Maximum principal strain: (a) monolithic specimen, (b) precast specimen

precast slab in situ topping, and the visualisation is shown in Fig. 19. The von-Mises stress of the reinforcement for the monolithic and the precast specimen is shown in Fig. 16. The principal strain is the indication of cracking in the specimen subjected to loading, as shown in Fig. 18.

**5.2 Load-displacement relationship**

Both the monolithic and the precast specimens were subjected to reverse cyclic loading similar to that of the experimental programme. Each displacement was applied three times, and the average load vs. displacement hysteresis graph at each displacement level of the

two specimens is shown in the Fig. 20. Even though ABAQUS cannot interpret for pinching effect (Mousavi *et al.*, 2014), it can accurately predict the capacity and the behaviour as similar to that of experimental testing. This graph also shows similar strength degradation in each cycle. The load vs. displacement hysteresis behaviour and the envelope graph for both specimens computed from the experimental and numerical results are shown in Figs. 21 and 22 respectively. The average difference in ultimate strength computed from finite element analysis and experiment is found to be less than 20%, which shows that the prediction of FEA is in close agreement with the test results.

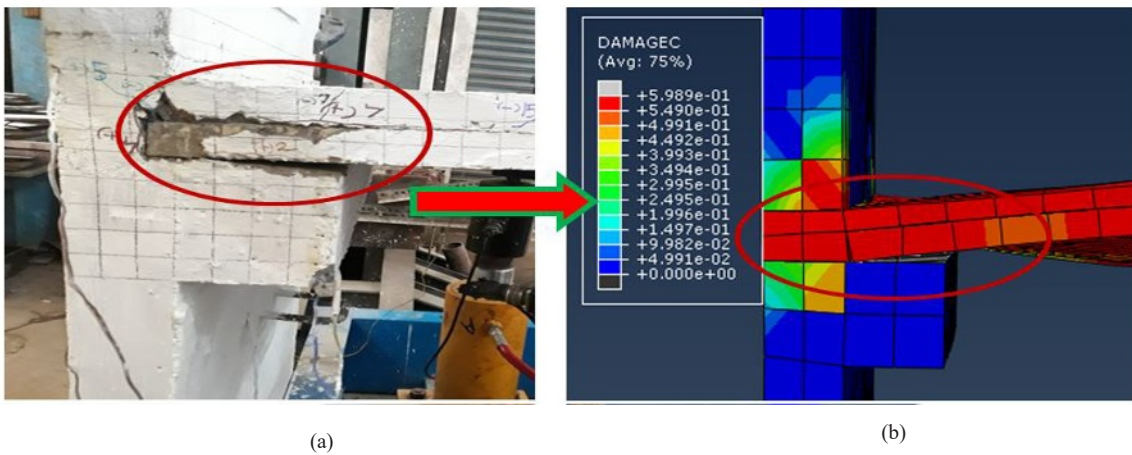


**Fig. 19** Separation of structural components in precast specimen: (a) experimental result, (b) ABAQUS result

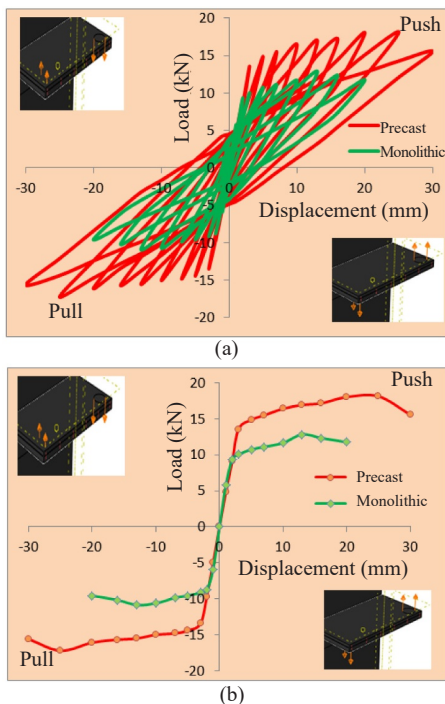


**Fig. 20** ABAQUS results: (a) hysteresis graph, (b) envelope curve

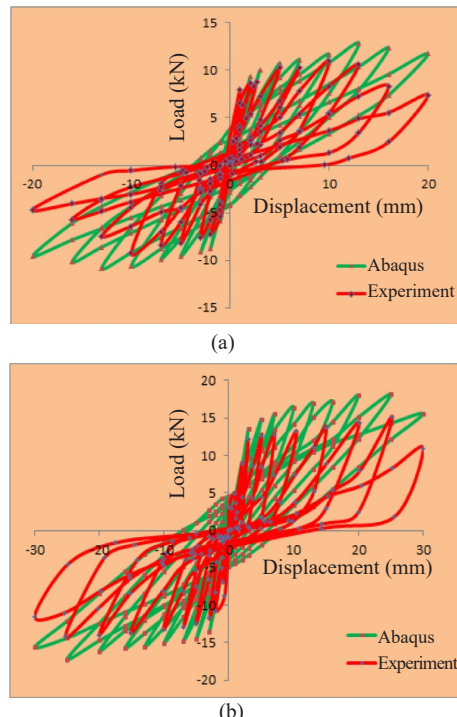


**Fig. 21** Comparison of numerical result with experimental result: (a) hysteresis behaviour of monolithic specimen, (b) hysteresis behaviour of precast specimen



### 5.3 Strength

The ultimate load-carrying capacities of the monolithic and precast specimens in the push and pull direction are shown in the Fig. 23. The load carrying capacity of the PS shows 41.6% and 58.4% greater than the MS in the push and pull direction, respectively. The precast specimen performs well when compared with the monolithic specimen.

### 5.4 Ductility

The ductility factor was calculated for both specimens (Table 8). The ductility factor from the finite element analyses for the precast specimen was found to be 66.51% greater than that of the monolithic specimen.

## 6 Result discussion

The shear wall-slab connection in structures generally anticipated for providing shear at the joint

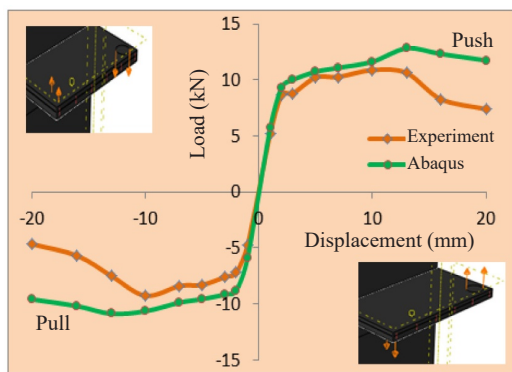
region. The reinforcement provided in the joint region should take care of shear forces acting at the connection region. Both the MS and PS meet the above expectations, but the ultimate shear strength was higher for PS due to the confinement provided in the joint region and the diaphragm action of the slab. The provision of U-shaped dowel bars from the precast shear wall lower panel and slab connected by the longitudinal reinforcement leads to the confinement in the joint region, and the diaphragm action is due to the screed concrete provided above the precast slab.

## 7 Conclusion

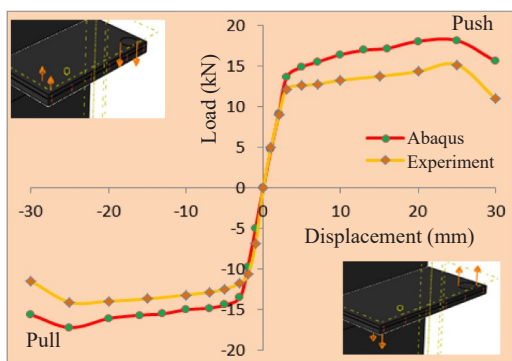
In this study, both experimental and numerical modelling was done to predict the structural performance of MS and PS subjected to reverse cyclic loading. The specimens were cast and modelled for a one-third scaled down model. Based on the experimental testing and analyses using the finite element model, the following

**Table 8 Comparison of ductility factor of the precast and monolithic specimen (ABAQUS)**

No.	Specimen type	Yield displacement $\Delta_y$ (mm)		Ultimate displacement $\Delta_u$ (mm)		Ductility factor, $\mu$		Average ductility factor, $\mu$
		Positive	Negative	Positive	Negative	Positive	Negative	
1	Monolithic	3.65	2.69	20	20	7.43	5.47	6.45
2	Precast	2.73	2.86	30	30	10.99	10.49	10.74

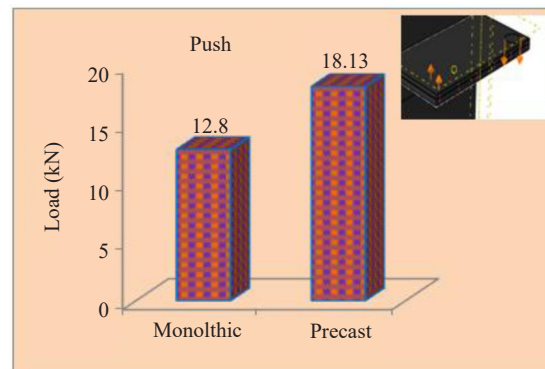


(a)

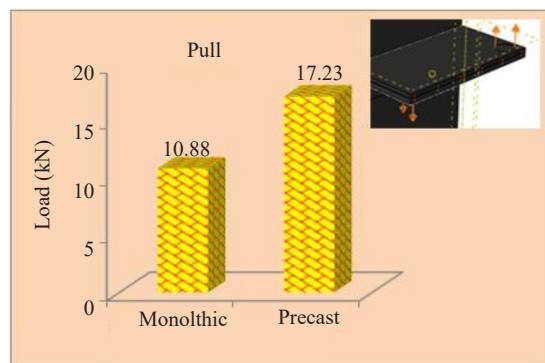


(b)

**Fig. 22 Comparison of numerical result with experimental result: (a) envelope curve of monolithic specimen, (b) envelope curve of precast specimen**



(a)



(b)

**Fig. 23 ABAQUS result: (a) ultimate load in push direction (b) ultimate load in pull direction**

observations are made.

(1) The experimental ultimate strength of PS was found to be 38.9% and 52.1% greater than the MS in the push and pull direction respectively. This is due to the presence of confinement in the joint core of the precast specimen and the diaphragm action of the precast slab. It was also found from FEA that the ultimate load for PS is 41.6% and 58.4% greater than the MS in the push and pull directions, respectively.

(2) The ultimate displacement reached by the PS and MS was about 30 mm and 20 mm, respectively. No visible crack was observed in the shear wall in both specimens. Only minor cracks formed in the nib portion of the precast specimen. The damage of the precast slab shows a similar trend as that of the monolithic specimen. A debonding between the structural members was observed in the precast specimen as displacement increased. The experimental load-displacement curve for the PS shows wider hysteresis behaviour and also shows good pinching effect due to the predefined gap between the connections.

(3) It was observed that, in the inelastic stage, the precast specimen showed higher stiffness when compared with the monolithic specimen. This is due to the additional stiffness provided by the presence of the nib supporting the precast slab in the PS.

(4) The average maximum load ratio for the MS and PS was found to be 1.31 and 1.25, respectively. The precast specimen was able to maintain the yield load for all the loading cycles up to 7.3% drift, but the reference MS showed a decreasing trend beyond 2.5% drift. The precast specimen exhibited less deterioration and performed well in the post-elastic stage.

(5) Considering the energy dissipation, the cumulative energy dissipation capacity of the PS was found to be 126.9% higher than that of the MS.

(6) It was observed that there was an increase in ductility for the PS of about 97.37% when compared with the MS, whereas there was an increase of about 66.51% for the PS when computed numerically. This proves that the precast dowel connection between the shear wall and slab behave in a ductile manner. The strain in the longitudinal reinforcement of the slab was found to be higher when compared with the strain in the vertical reinforcement of the wall for both the monolithic and precast specimens, which shows slab mode failure.

(7) The proposed numerical model accurately predicts the response of the joint assemblage concerning failure, deformation and strain responses of the specimens. This model can also be used for estimating the shear resistance of precast dowel connections. The average difference in ultimate load carrying capacity of joint computed both numerically and experimentally is less than 20%, which shows that the prediction of FEA is in close agreement with the test results. The interaction between the structural components and the damage parameter plays an important role in the modelling of precast structures.

(8) It is concluded that the provision of dowels as shear reinforcement in the precast shear wall-slab joint region would be effective in seismic risk regions.

## Acknowledgement

This research work was supported by the Council of Scientific & Industrial Research (CSIR), New Delhi, India. The authors are thankful to the funding agency for their support.

## References

- Alameddine F and Eshani MR (1991), "High Strength RC Connections Subjected to Inelastic Cyclic Loading," *ASCE Journal of Structural Engineering*, **117**(3): 829–850.
- Alfarah B, Lopez-Almansa F and Oller S (2017), "New Methodology for Calculating Damage Variables Evolution in Plastic Damage Model for RC Structures," *Engineering Structures*, **132**: 70–86.
- Dere Y and Koroglu MA (2017), "Nonlinear FE Modeling of Reinforced Concrete," *International Journal of Structural and Civil Engineering*, **6**(1): 71–74.
- Elliot KS (2017), *Precast Concrete Structure*, Second Edition, CRC press, Taylor & Francis, New York.
- Feng B, Xiong F, Liu B, Chen J and Zhang Y (2016), "Shear Performance of Horizontal Joints in Short Precast Concrete Columns with Sleeve Grouted Connections under Cyclic Loading," *PLOS ONE*, **11**(11): e0165988.
- Fib Fédération Internationale du Béton (2013), *Model Code 2010*, Vol. 1 & 2, Bulletin No. 65 & 66.
- Fischinger M, Zoubek B, Kramar M and Isakovic T (2012), "Cyclic Response of Dowel Connections in Precast Structures," *15th World conference on Earthquake Engineering*, Lisbon, Portugal.
- Greeshma S and Jaya KP (2008), "Seismic Behaviour of Shear Wall-Slab Connection," *Proceeding 14th World Conference on Earthquake Engineering*, Beijing, China, 12–17.
- Greeshma S and Jaya KP (2011), "Effect of Slab Shear Reinforcement on the Performance of Shear Wall-Floor Slab Connection," *Journal of Performance of Constructed Facilities*, *ASCE*, **27**(4): 391–401.
- Greeshma S and Jaya KP (2012), "Effect of Cross Inclined Bars on the Behaviour of Shear Wall-floor Slab Joint under Lateral Cyclic Loading," *Journal of Structural Engineering*, **39**(1): 9–14.
- Greeshma S, Jaya KP and Rajesh C (2012), "Seismic Behaviour of the Shear Wall-Slab Joint under Lateral Cyclic Loading," *Asian Journal of Civil Engineering (Building and Housing)*, **13**(4): 455–464.
- Han W, Zhao Z, Qian J, Zhang Y and Ma T (2019), "Experimental Seismic Behavior of Squat Shear Walls

- with Precast Concrete Hollow Moulds,” *Earthquake Engineering and Engineering Vibration*, **18**(4): 871–886.
- Hutchinson RLP, Rizkalla SH, Lau M and Heuvel SP (1991), “Horizontal Post-Tensioned Connections for Precast Concrete Load-Bearing Shear Wall Panels,” *PCI Journal*, **36**(6): 64–76.
- IS 1893 (Part 1): 2002 (2002), *Indian Standard Criteria for Earthquake Resistant Design of Structures*, Bureau of Indian Standards, New Delhi, India.
- IS 456-2000 (2000), *Indian Standard Plain and Reinforced Concrete Code of Practice*, Bureau of Indian Standards, New Delhi, India.
- IS 13920-1993 (1993), *Indian Standard Ductile Detailing of Reinforced Concrete Structures Subjected to Seismic Forces*, Bureau of Indian Standards, New Delhi, India.
- Joshi MK, Murty CVR and Jaisingh MP (2005), “Cyclic Behaviour of Precast RC Connections,” *The Indian Concrete Journal*, **79**(11): 43–50.
- Kaushika S and Dasgupta K (2015), “Seismic Damage in Shear Wall-Slab Junction in RC Buildings,” *Proceedings of the 12th International Conference on Vibration Problems, Science Direct, Procedia Engineering*, **144**: 1332–1339.
- Kaushika S and Dasgupta K (2019), “Seismic Behaviour of Slab – Structural wall Junction of RC Buildings,” *Earthquake Engineering and Engineering Vibration*, **18** (2): 331–349.
- Ketiyot R and Hansapinyo C (2018), “Seismic Performance of Interior Precast Concrete Beam-Column Connections with T-Section Steel Inserts under Cyclic Loading,” *Earthquake Engineering and Engineering Vibration*, **17**(2): 355–369.
- Kremmyda GD, Fahjan YM and Psycharis IN (2013), “Analytical Prediction of the Shear Resistance of Precast RC Pinned Beam-to-Column Connections,” *4th ECCOMAS Thematic Conference on Computational Methods in Structural Dynamics and Earthquake Engineering*, Kos Island, Greece.
- Lu X, Yang B and Zhao B (2018), “Shake-Table Testing of a Self-Centering Precast Reinforced Concrete Frame with Shear Walls,” *Earthquake Engineering and Engineering Vibration*, **17**(2): 221–233.
- Magliulo G, Ercolino M, Cimmino M, Capozzi V and Manfredi G (2014), “Seismic Behavior of Beam-to-Column Dowel Connections: Numerical Analysis vs Experimental Test,” *Second European Conference on Earthquake Engineering and Seismology*, Istanbul, 25–29.
- Mousavi SA, Zahrai SM, and Bahrami-Rad (2014), “Quasi-static Cyclic Tests on Super-lightweight EPS Concrete Shear Walls,” *Engineering Structures*, **65**: 62–75.
- Obaidat YT, Heyden S and Dahlblom O (2010), “The Effect of CFRP and CFRP/Concrete Interface Models When Modelling Retrofitted RC Beams with FEM,” *Composite Structures*, **92**: 1391–1398.
- Rahman AB, Leong DCP, Saim AA and Osman MH (2006), “Hybrid Beam-to-Column Connections for Precast Concrete Frames,” *Proceedings of the 6th Asia-Pacific Structural Engineering and Construction Conference*, Kuala Lumpur, Malaysia.
- Rossley N, Aznieta Abdul Aziz FN and Chew HC (2014), “Behaviour of Precast Walls Connection Subjected to Shear Load,” *Journal of Engineering Science and Technology*, Special issue **10**: 142–150.
- Saqan EI (1995), “Evaluation of Ductile Beam Column Connections for Use in Seismic Resistant Precast Frames,” *PhD Thesis*, University of Texas, Austin.
- Seifi P, Henry RS and Ingham JM (2015), “Preliminary Test Results of Precast Concrete Panels with Grouted Connections,” *2015 NZSEE Conference*, 744–751.
- Soudki KA, West JS, Rizkalla SH, Blackett B and Eng P (1996), “Horizontal Connections for Precast Concrete Shear Wall Panels under Cyclic Shear Loading,” *PCI Journal*, **41**: 64–80.
- Surumi RS, Jaya KP and Greeshma S (2015a), “Numerical Evaluation of Structural Wall-Flat Slab Connection,” *Gradevinar*, **67**(7): 663–672.
- Surumi RS, Jaya KP and Greeshma S (2015b), “Modelling and Assessment of Shear Wall-Flat Slab Joint Region in Tall Structures,” *Arabian Journal for Science and Engineering*, **40**: 2201–2217.
- Tawfik AS, Badr MR and ElZanaty A (2014), “Behavior and Ductility of High Strength Reinforced Concrete Frames,” *Housing and Building National Research Center, HBRC Journal*, **10**(2): 215–221.
- Vaghei R, Hejazi F, Taheri H, Jaafar MS and Aznieta Abdul Aziz FN (2017), “Development of a New Connection for Precast Concrete Walls Subjected to Cyclic Loading,” *Earthquake Engineering and Engineering Vibration*, **16**(1): 97–117.
- Yuksel E, Karadogan HF, Bal IE, Ilki A, Bal A and Inci P (2015), “Seismic Behavior of Two Exterior Beam-Column Connections Made of Normal-strength Concrete Developed for Precast Construction,” *Engineering Structures*, **99**: 157–172.
- Zenunovic D and Folic R (2012), “Models for Behaviour Analysis of Monolithic Wall and Precast or Monolithic Floor Slab Connections,” *Engineering Structures*, **40**: 466–478.
- Zhao Q, Zhang Z, Liu J and Chu M (2014), “Experimental Study on Precast Concrete Shear Walls with Different Hollow Slabs,” *The Open Civil Engineering Journal*, **8**: 166–171.
- Zoubek B, Fahjan Y, Fischinger M and Isakovic T (2014), “Nonlinear finite element modelling of centric dowel connections in precast buildings,” *Computers and Concrete*, **14**(4): 463–477.